Journal of Materials Science: Materials in Electronics (2019) 30:16922–16931
https://doi.org/10.1007/s10854-019-01639-9

Development of highly luminescent PMMA films doped with Eu^{3+}β-diketonate coordinated on ancillary ligand

L. H. C. Francisco[1] · M. C. F. C. Felinto[1] · H. F. Brito[2] · E. E. S. Teotonio[3] · O. L. Malta[4]

Received: 21 March 2019 / Accepted: 31 May 2019 / Published online: 11 June 2019

Abstract

In this work, $[Eu(tta)_3(4\text{-picNO})_2]$ and $[Eu(dbm)_3(4\text{-picNO})]$ complexes were incorporated on different concentrations (x = 1, 3, 5, 10 and 15%) in PMMA polymeric matrix (4-picNO: 4-Methylpyridine N-oxide) by the solvent casting method, yielding transparent and highly luminescent polymeric films. These materials were analyzed by X-ray diffraction, scanning electron microscopy and by energy dispersive, ultraviolet–visible spectroscopy, luminescence and vacuum ultraviolet–ultraviolet spectroscopies. The luminescence spectra of doped PMMA films are in agreement with an efficient intramolecular diketonate (tta) ligand-to-europium energy transfer. Furthermore, the values of experimental intensity parameters ($\Omega_{2,4}$) for luminescent polymeric materials were quite similar to those ones for isolated complexes, indicating that there is a homogeneous dispersion of Eu^{3+} complexes in the polymeric matrix, preserving their chemical and structural features. These behavior were also observed from the CIE diagram that show great similarity between the (*x,y*) coordinates for the doped PMMA samples compared to the isolated β-diketonate complexes with a reddish color tuning. The photostability investigation of the doped PMMA polymeric films and Eu^{3+} complexes has been also reported.

1 Introduction

Interest in a variety of luminescent materials containing trivalent rare earth (RE^{3+}) ions as emitting centers has grown significantly in recent years due to their electronic structures. However, their unique spectroscopic and magnetic properties emerge with distinguished importance when developing new materials for a wide variety of application fields [1–3]. The spectroscopic properties of RE^{3+} ions are inclined towards developments to luminescent markers [4], LEDs and OLEDs lighting devices [5], upconversion [6], solar cells sensitizers [7–9], as well as temperature sensing [10] and luminescent probes to biomolecules [11].

The 4f electrons interact weakly with the environment, resulting in little variance on the energy level structure on RE^{3+} ions. Therefore, the absorption and emission spectra of rare earth compounds exhibit narrow bands derived from 4f-4f transitions in solution or solid state, which facilitates the interpretation of these spectroscopic data [12]. The molar absorption coefficients of the 4f-intraconfigurational transitions are very low because they are forbidden by Laporte's rule [13]. However, several RE^{3+} complexes often showcase a very strong luminescence arising from the metal ion. This phenomenon is explained by intramolecular energy transfer (ET) process from the organic ligand excited states to the RE^{3+} energy levels [13].

Besides, the Eu^{3+} ions are often used as a spectroscopic probe regarding the structural and photoluminescence properties [14]. As the first excited state ($^5D_0$) and the fundamental state ($^7F_0$) are non-degenerate, it greatly facilitates the analysis of experimental luminescence spectra. Moreover, $^5D_0 \rightarrow {}^7F_J$ transitions with low J values and well separated $^5D_0 \rightarrow {}^7F_J$ lines further aid spectral interpretation.

In this scenario, β-diketonate complexes have been largely employed due to their high molar absorptions and

Electronic supplementary material The online version of this article (https://doi.org/10.1007/s10854-019-01639-9) contains supplementary material, which is available to authorized users.

✉ M. C. F. C. Felinto
mfelinto@ipen.br

1 Nuclear and Energy Research Institute, IPEN/USP, Sao Paulo, SP, Brazil

2 Institute of Chemistry, University of São Paulo, Sao Paulo, SP, Brazil

3 Department of Chemistry, Federal University of Paraíba, Joao Pessoa, PB, Brazil

4 Department of Fundamental Chemistry, Federal University of Pernambuco, Recife, PE, Brazil

the position of the ligand triplet states (T_1), which are slightly above the emitting excited levels of RE^{3+} ions, leading to an efficient luminescence sensitization. In addition, the photoluminescence processes can be supported by ancillary ligands with absence of high energy oscillators (i.e. vibrionic O–H oscillators present in hydrated complexes) that minimize the non-radiative contributions [12, 14].

Several RE^{3+} compounds present low thermal stability, limited photostability and poor mechanical properties. However, a potential approach to incorporate those complexes into organic polymers may solve most of these deficiencies, providing additional advantages such as flexibility, optical quality and moderate processing conditions [2, 15–17].

Poly(meyhylmethacrylate) (PMMA) polymer is widely known for its high light transmittance, chemical resistance, refractive index tailorability, low optical absorption and UV resistance. PMMA embedding organic and inorganic particles have been used to improvement of electrical conductivity, photoconductivity, photoluminescence, photo-induced charge-transfer and magnetic properties. [18–24].

In this work, $[Eu(dbm)_3{\cdot}4\text{-picNO}]$ and $[Eu(tta)_3(4\text{-picNO})_2]$ complexes were synthesized by the precipitation method and further incorporated into PMMA polymeric film in different concentrations (x = 1, 3, 5, 10 and 15%) via solvent casting. The doped PMMA materials show high luminescence intensities, under UV irradiation. The experimental intensity parameters (Ω_λ) for the complexes and doped systems are discussed. These novel luminescent Eu^{3+} materials may act as light converting molecular devices. The photostability of the doped PMMA polymeric films are higher than for the individual Eu^{3+} complexes. The generation of new light emitters with range color coordinates (x, y) for application as optical markers is presented.

2 Experimental section

2.1 Synthesis

All materials used in this work were purchased from Synth, VETEC, CAAL and Sigma-Aldrich and used without further purification. The purity of reagents follows: Ethyl alcohol (99.5%); Chloroform, anhydrous, contains amylenes as stabilizer (99%); Acetone (99.5%); Ammonium hydroxide solution 28.0–30.0% NH_3 basis; 1,3-Diphenyl-1,3-propanedione or dibenzoylmethane (98%); 2-Thenoyltrifluoroacetone (99%); 4-Methylpyridine N-oxide (4-picNO) (98%); Europium(III) chloride hexahydrate (99,9%); Poly(methyl methacrylate) powder, analytical standard, average molecular weight of 78,000 g/mol by GPC (gel permeation chromatography).

2.1.1 Synthesis of $Eu(\beta\text{-diketonate})_3{\cdot}y(H_2O)$ complexes

The hydrated europium β-diketonate complexes were carried out by the dissolution of dibenzoylmethane (dbm) or thenoyltrifluoroacetone (tta) in ethanol at 50 °C, followed by the dropwise addition of NH_4OH until neutral pH was reached. The solutions were kept under constant stirring as the following addition of a stochiometric amount of an $EuCl_3{\cdot}6H_2O$ aqueous solution lowered the pH of the mixture. NH_4OH was further added to neutralize pH once again. The mixtures were kept under stirring for 2 h until the precipitation of a characteristic yellowish solid. These compounds were then filtered and dried under reduced pressure in vacuum desiccator.

2.1.2 Synthesis of $Eu(\beta\text{-diketonate})_3{\cdot}y(4\text{-picNO})$ complexes

This step aims to substitute water molecules in the Eu^{3+} coordination polyhedron of the previously synthesized hydrated complexes by 4-picoline-N-oxide (4-picNO) ligand. Thus, acetone solutions of Eu^{3+}(dbm or tta) hydrated complexes were kept under stirring while a stoichiometric volume of 4-picNO acetone solution with defined concentration was added dropwise to the mixture. The precipitate powder was obtained by solvent evaporation and further dried under reduced pressure in vacuum desiccator.

2.1.3 Preparation of $PMMA:[Eu(tta)_3(4\text{-picNO})_2]$ (x%) films

The preparation of the luminescent doped polymeric films was carried out by the solvent casting method. Firstly, a set amount of PMMA was kept under stirring in chloroform at 60 °C for 1 h. After the polymer dissolved, an acetone solution containing the stoichiometric amount of the previously synthesized $[Eu(diketonate)_3{\cdot}y(4\text{-picNO})]$ (diketonate: tta or dbm) was added in the mixture, which was stirred for an additional hour at 60 °C. The mixture was then transferred to a Petri dish, where the polymer film was obtained after evaporation of excess solvent at 40 °C (Fig. 1). The same procedure was used for several doping different concentrations of each Eu^{3+} β-diketonate complexes where x = 1, 3, 5, 10 and 15% weight for $PMMA:[Eu(tta)_3(4\text{-picNO})_2](x\%)$ labeled as PET1, PET3, PET5, PET10 and PET15 and for $PMMA:[Eu(dbm)_3(4\text{-picNO})](x\%)$ labeled as PED1, PED3, PED5, PED10 and PED15, respectively.

2.2 Instrumental

Scanning electron microscopy (SEM) measurements were performed on HITACHI TM3000 microscope at 5 and 15 kV acceleration voltages in charge-up reduction mode, while Energy Dispersive Spectroscopy (EDS) data was obtained through a XFlash 430H detector and processed by

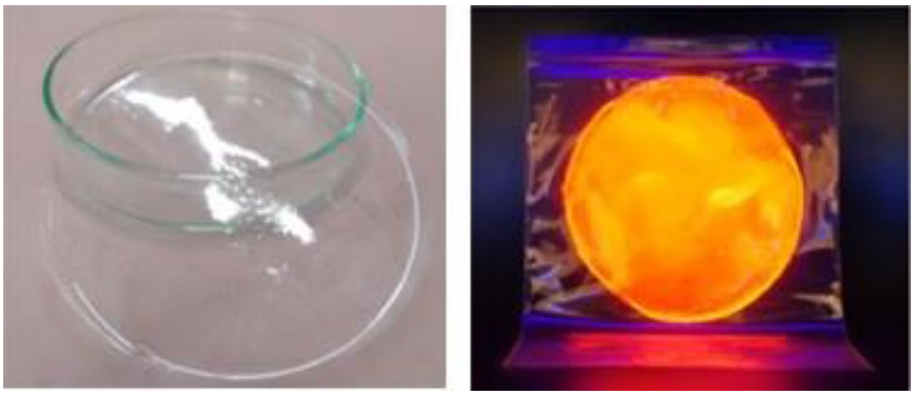

Fig. 1 PMMA:[Eu(dbm)$_3$(4-picNO)](5%) doped film taken with a digital camera displaying the red emissions under visible light (left) and UV irradiation at 366 nm (right)

Quantax70 software on the same equipment. X-Ray Diffraction (XRD) patterns were obtained by $K\alpha_{Cu}$ radiation on a Rigaku Miniflex II diffractometer. Measurements were made on the 5–80°(2θ) range, using a 0.03° step width under 1 s count time, as well as a 30 kV voltage and a 15 mA current. Ultraviolet–visible absorption spectroscopy (UV–vis) data were acquired by a Shimadzu UV-2600 spectrophotometer in the spectral range of 200 to 600 nm. Standard luminescence analysis was performed on a HORIBA Fluorog-3 Spectrofluorimeter and processed by FluorEssence software. Spectral acquisition was measured by an axial setup at an angle of 22.5° with slit widths of 0.5–1.0 nm and a blazed holographic grating 1200 lines/mm. Emission spectra was registered through a CCD detector while excitation spectra were measured by a photomultiplier with 1 nm step width. Synchrotron radiation measurements were obtained at the Brazilian Synchrotron Light Laboratory (LNLS), on TGM (Toroidal Grating Monochromator) beamline, which is dedicated to ultraviolet spectroscopy techniques in the energy range of 3 to 330 eV. Vacuum Ultraviolet to Ultraviolet (VUV-UV) spectroscopy was performed at room temperature within the 4.5–7.5 eV range, using a 200 nm thick quartz slide to avoid second order harmonics from the beamline. The resulting signal was collected by an optical fiber and further corrected applying sodium salicylate as a standard reference.

3 Results and discussion

3.1 Characterization

SEM images of the (a) [Eu(tta)$_3$(4-picNO)$_2$] and the [Eu(dbm)$_3$(4-picNO)] complexes, PED3 and PET3 samples show distinguishable dispersion throughout the polymer from the microstructures, where it is noticeable the existence of complex aggregates in higher magnification images (Fig. 2). Moreover, it is plausible to assume a similarity in dimension sizes between the particle distribution on polymer samples and on isolated Eu^{3+}β-diketonate complexes. Additionally, it is possible to observe the typical porous morphology regarding amorphous PMMA in high magnification of polymer samples.

EDS density maps in Fig. 3 indicate a successful dispersion of the β-diketonate complexes throughout the polymer, containing carbon, oxygen and europium. The europium imaging (Fig. 3d) suggest that Eu complexes are incorporate homogeneously in PMMA polymer matrix.

X-ray diffraction patterns display broadened diffraction peaks, revealing samples of an amorphous nature as expected for PMMA polymeric systems (Fig. 4). Furthermore, there are no significant changes in the diffraction pattern profiles of the polymer when increasing the doped concentration of both [Eu(tta)$_3$(4-picNO)$_2$] and the [Eu(dbm)$_3$(4-picNO)] complexes from 1, 3, 5, 10 and 15% is seemingly identical on all analyzed samples, regardless of the doping β-diketonate complex.

3.2 Spectroscopic properties

UV–Vis absorption spectra of the PMMA, PET1 and PED1 samples present a clear distinction in the among the broad absorption bands (at around 225, 270 and 345 nm) originated from the β-diketonate ligands in the Eu^{3+} complexes and PMMA polymer (Fig. 5). The absorption spectral profiles of doped samples strongly differ from isolated PMMA, showing that the PET1 and PED1 samples present higher absorption intensity than for PMMA polymeric matrix. Moreover, it is shown that the coordination of the 4-picNO ligand does not result in any spectral changes compared to know europium β-diketonate coordination compounds, as its absorption range lies within the range of β-diketonate ligands, such as indicated by the absorption spectra.

VUV-UV excitation spectra by synchrotron radiation of the PMMA and doped films (PET10 and PED10) were recorded in the energy range from 4.5 to 7.5 eV (276–165 nm). The results show a qualitative understanding of ligand absorption processes at high energy (Fig. 6).

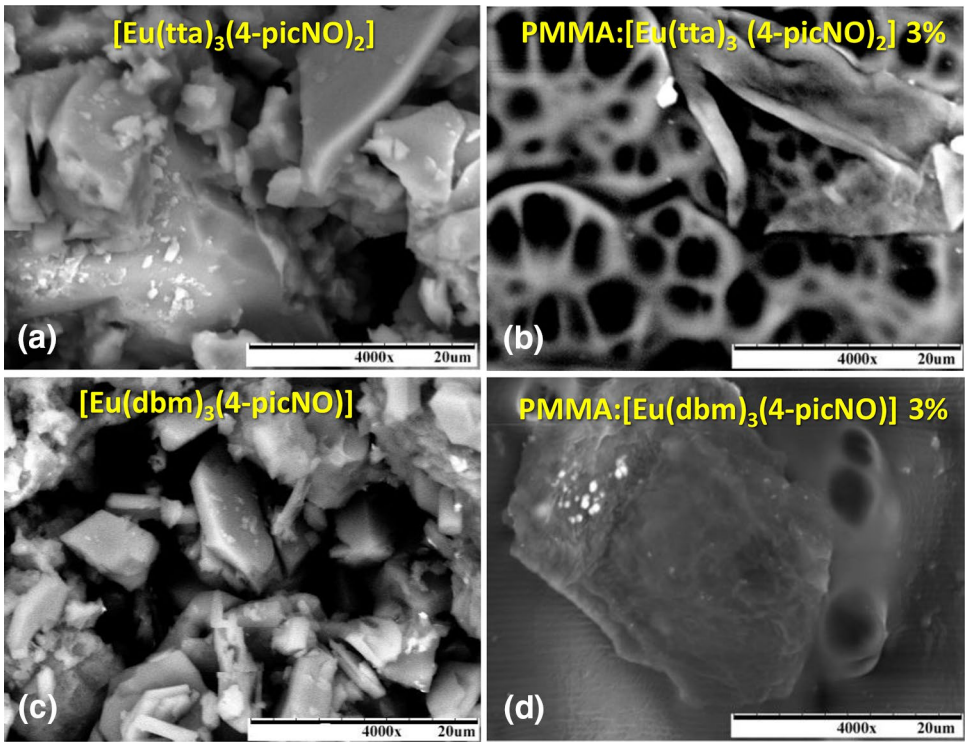

Fig. 2 SEM images of the samples under × 4000 magnification of **a** $[Eu(tta)_3(4\text{-picNO})_2]$, **b** PMMA:$[Eu(tta)_3(4\text{-picNO})_2]$ (3%), **c** $[Eu(dbm)_3(4\text{-picNO})]$ and **d** PMMA:$[Eu(dbm)_3(4\text{-picNO})]$(3%)

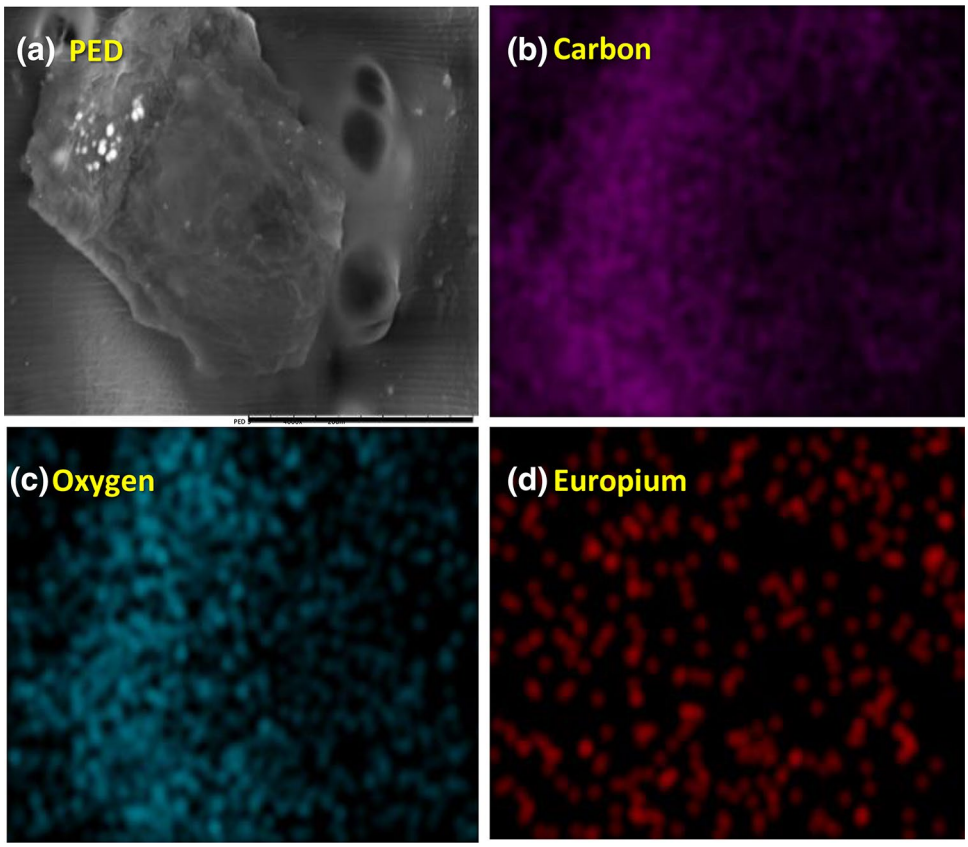

Fig. 3 EDS density maps of samples of **a** PMMA:$[Eu(dbm)_3(4\text{-picNO})]$ (3%) (PED3) **b** Carbon (K), **c** Oxygen (K) and **d** Europium (L) distributions

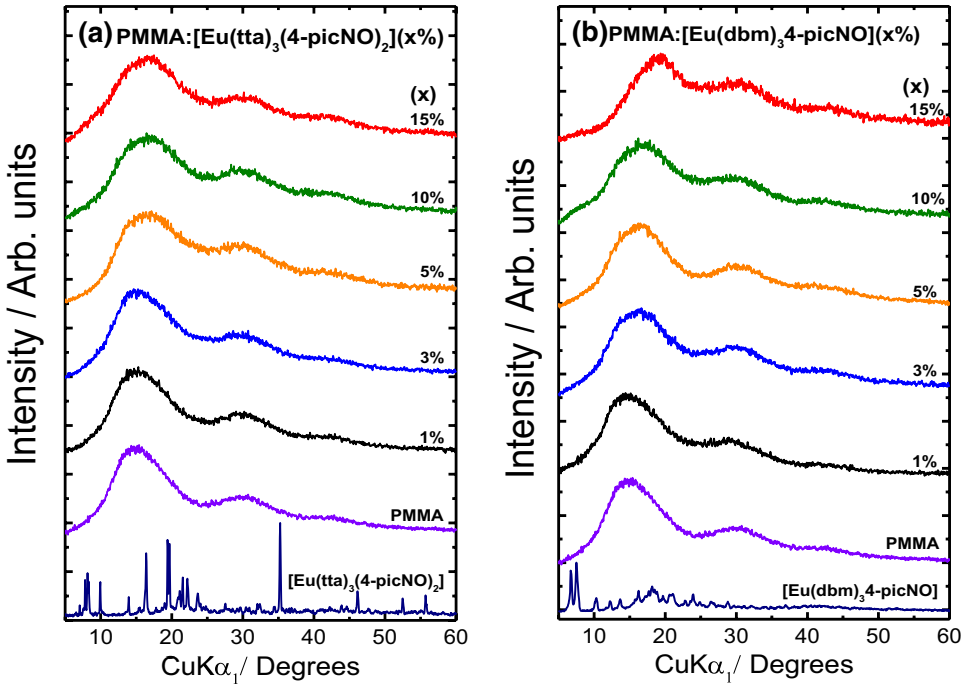

Fig. 4 XRD patterns of **a** PMMA:[Eu(tta)$_3$(4-picNO)$_2$](x %) and **b** PMMA:[Eu(dbm)$_3$(4-picNO)] (x %) films varying doping concentration from 1 to 15%

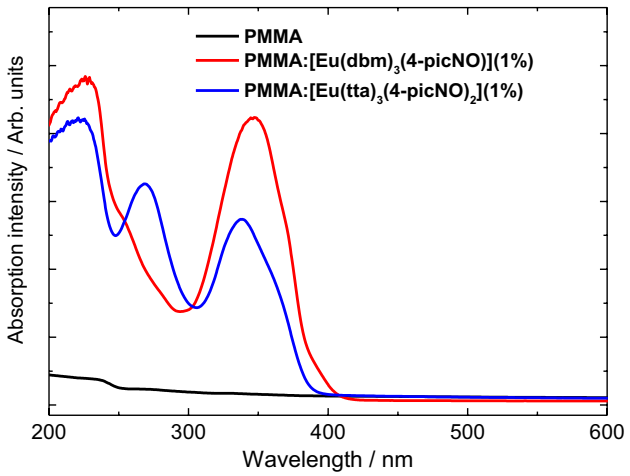

Fig. 5 Absorption spectra of PMMA polymer, PMMA:[Eu(dbm)$_3$(4-picNO)](1%) and PMMA:[Eu(tta)$_3$(4-picNO)$_2$](1%) recorded in the spectral range of 200 to 600 nm

As it can be seen, the excitation spectra of doped polymer samples presented a much higher absorption rate compared with PMMA matrix.

In addition, VUV-UV emission spectra present the same $^5D_0 \rightarrow {}^7F_J$ transitions (J = 1, 2, 3, 4) under excitation at higher energies without any noticeable emission spectral changes (Fig. 6a–b). However, higher emission intensity of the 4f-4f transitions in the visible region are directly correlated to higher absorption energy illustrated in 3D spectra. This optical feature is observed for the PED10 doped film that presented maxima absorption bands around 4.5, 4.7, 5.2 and 6.4 eV, as well as for PET10 doped film shows higher absorption bands at 4.5, 4.7 and 6.0 eV.

Excitation spectra of PMMA:[Eu(tta)$_3$(4-picNO)$_2$](x%) and PMMA:[Eu(dbm)$_3$(4-picNO)](x%) films (x = 1, 3, 5, 10 and 15%), monitoring on Eu^{3+} hypersensitive transition (~ 612 nm) were recorded at room temperature (300 K), in Fig. 7. The broad absorption bands are attributed to the intraligand transitions ($S_0 \rightarrow S_n$) [13] in the range of 200 to 425 nm. In addition, it is observed the narrow absorption with the lowest intensity assigned to $^7F_0 \rightarrow {}^5D_2$ transition [14]. It is noticeable that the excitation spectra presents higher absorption intensity bands centered on the ligand compared to 4f-4f transitions, indicating its potential to act as an antenna on energy-transfer processes to Eu^{3+} ions. The comparison between the excitation spectra of 4-picNO and the hydrated europium of β-diketonate complexes reveals that the ancillary ligand coordination leads to the different excitation spectral profiles from the broad absorption bands assigned the $S_0 \rightarrow S_n$ transitions (Figure S1).

Emission spectra of PMMA:[Eu(tta)$_3$(4-picNO)$_2$](x%) and PMMA:[Eu(dbm)$_3$(4-picNO)](x%) films were recorded at 300 K, under excitation at $^7F_0 \rightarrow {}^5L_6$ transition (394 nm) of Eu^{3+} ion, which show the narrow emission bands attributed to $^5D_0 \rightarrow {}^7F_J$ (J = 0, 1, 2, 3 and 4) transition (Fig. 8) [14]. Among these optical data, the $^5D_0 \rightarrow {}^7F_0$ transition is of extreme importance since it can indicate the number of symmetry sites around europium ions. However, the $^5D_0 \rightarrow {}^7F_1$ transition is allowed my magnetic dipole, thus formally insensible to the chemical environment around the Eu^{3+} ion. In addition, the hypersensitive $^5D_0 \rightarrow {}^7F_2$ and $^5D_0 \rightarrow {}^7F_4$ transitions is deeply affected by the surrounding ligand field,

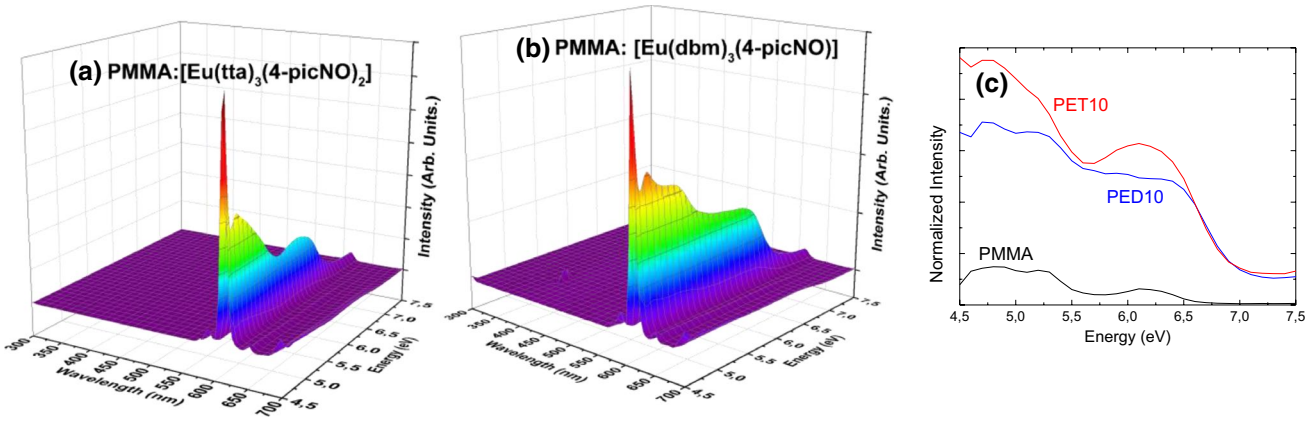

Fig. 6 3D emission spectra recorded under VUV-UV excitation for samples: **a** PET10 and **b** PED 10 measured at room temperature. **c** VUV-UV absorption spectra of PMMA doped films recorded at room temperature

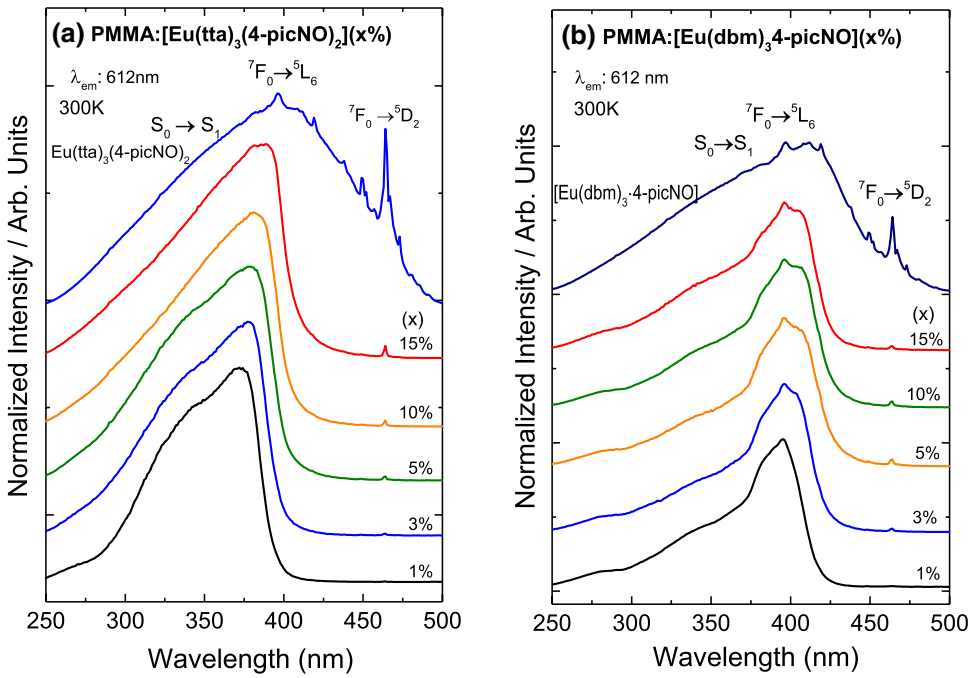

Fig. 7 Excitation spectra recorded at 300 K monitored at 612 nm of **a** PMMA:[Eu(tta)$_3$(4-picNO)$_2$](x %) and the **b** PMMA:[Eu(dbm)$_3$(4-picNO)] (x %) films varying doping concentration from 1 to 15%

as their emission intensity varies highly according to Eu^{3+} symmetry site.

Thus, a presence of the highest emission intensity bands assigned to $^5D_0 \rightarrow {}^7F_2$ transition indicate that Eu^{3+} ions occupy non-centrosymmetric sites for all samples (Fig. 8). Moreover, the emission bands from $^5D_0 \rightarrow {}^7F_0$ transition show only one emission peak, suggesting that the Eu^{3+} ion occupies just one single site of symmetry on PMMA samples. It is also noted that broad emission bands were not observed on spectral range from 450 to 600 nm (Fig. 8), indicating an efficient energy transfer from β-diketonates and 4-picNO organic ligands to the Eu^{3+} ion. Therefore, the Eu^{3+} coordination of the 4-picNO ligand is relevant regarding luminescence intensity, acting as an efficient antenna for energy transfer processes and prevents non-radiative decay channel due to OH oscillators from the hydrated complexes. In addition, the 4-picNO ligand exhibits different emission spectral profiles manly from the $^5D_0 \rightarrow {}^7F_2$ transitions, indicating different chemical environment around europium ion due to different ligand field interaction in each coordination compound. Also, the coordination of the ancillary ligand enhances the energy transfer processes of Eu^{3+} complexes (Figure S1).

The experimental intensity parameters (Ω_λ) consider the simultaneous contributions from forced electric dipole and dynamic coupling mechanisms and may be obtained from 4f-4f transitions in the absorption or emission spectra [12, 13]. The experimental intensity parameters Ω_2 and Ω_4 were

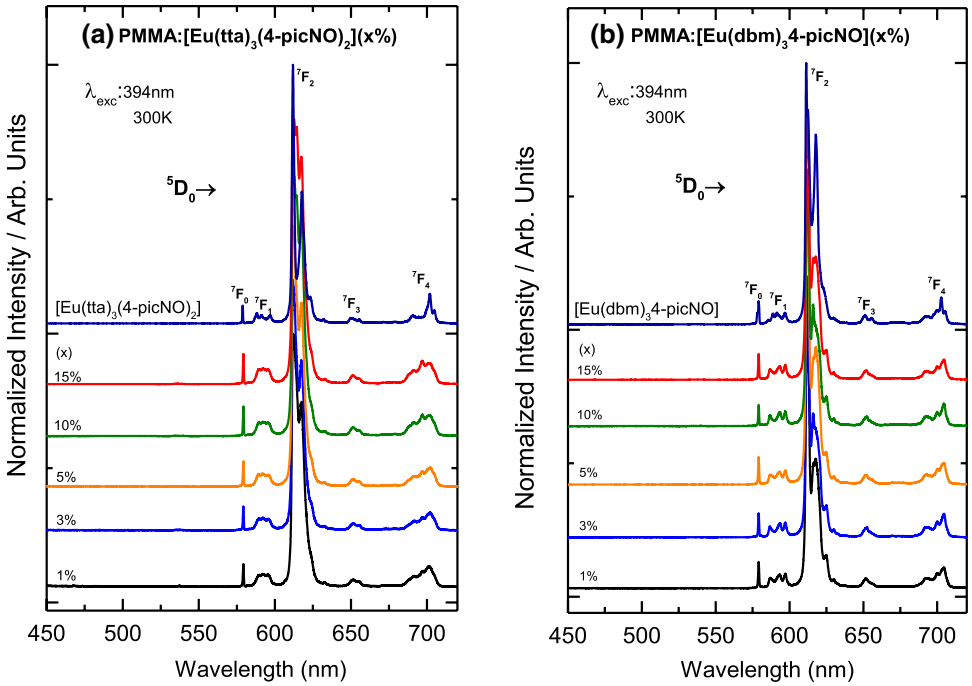

Fig. 8 Emission spectra recorded at 300 K under excitation at 394 nm of **a** PMMA:[Eu(tta)$_3$(4-picNO)$_2$](x %) and the **b** PMMA:[Eu(dbm)$_3$(4-picNO)] (x %) films varying doping concentration from 1 to 15%

determined for the [Eu(tta)$_3$(4-picNO)$_2$] and [Eu(dbm)$_3$(4-picNO)] complexes, as well as for doped PMMA samples, in which, emission intensity is given in terms of the area under the curve of $^5D_0 \rightarrow {}^7F_J$ transitions, being defined as:

$$I_{0\rightarrow J} = \hbar\omega_{0\rightarrow J} A_{0\rightarrow J} N_0 \quad (1)$$

where $\hbar\omega_{0\rightarrow J}$ corresponds to the transition's energy, N_0 is the population of the emitting level ($^5D_0$), and $A_{0\rightarrow J}$ represents the coefficient of spontaneous emission (emission intensity measured as emitted power; however, actually most equipment measures the ratio between absorbed and emitted number of photons). For experimental determination of the rates $A_{0\rightarrow J}$,. the $^5D_0 \rightarrow {}^7F_1$ transition allowed by magnetic dipole was used as standard reference, since it is formally insensitive to the chemical environment [12]. Thus, $A_{0\rightarrow J}$ values are obtained from:

$$A_{0\rightarrow J} = \left(\frac{S_{0\rightarrow J}}{S_{0\rightarrow 1}}\right) A_{0\rightarrow 1} \quad (2)$$

where $S_{0\rightarrow J}$ is the area (integrated intensity) under the curve of the corresponding $^5D_0 \rightarrow {}^7F_J$ transition of the $^5D_0 \rightarrow {}^7F_1$ and $^5D_0 \rightarrow {}^7F_{2,4}$ transitions. Hence, Ω_λ ($\lambda = 2, 4$) presented on Table 1 were calculated from the following equation:

$$A_{0\rightarrow J} = \frac{4e^2\omega^3}{3\hbar c^3} \frac{1}{2J+1} \chi \sum_{\lambda=2,4} \Omega_\lambda \langle {}^5D_0 \parallel U^{(\lambda)} \parallel {}^7F_J \rangle^2 \quad (3)$$

where $\chi = n_0\left(n_0^2 + 2\right)^2/9$ is the Lorentz local field correction, and n_0 is as the material's refractive index. The squared reduced matrix elements are tabulated in the literature as 0.0032 and 0.0023 for J = 2 and 4, respectively.

The Ω_2 and Ω_4 experimental intensity parameter values of the [Eu(tta)$_3$(4-picNO)$_2$] complex compared with those doped polymer system (PET1, PET3, PET5, PET10 and PET15) as well as for [Eu(dbm)$_3$(4-picNO)] compound compared with those PED1, PED3, PED5, PED10 and PED15 systems are quite similar (Table 1). These spectroscopic results suggest that the Eu^{3+} complexes maintain their chemical and structural features in the first coordination sphere when doped in PMMA polymeric film. indicating that the europium complexes do not interact straightly with the polymer in the first coordination sphere, but they are

Table 1 Experimental values of intensity parameters ($\Omega_{2,4}$) determined from the $^5D_0 \rightarrow {}^7F_0$ and $^5D_0 \rightarrow {}^7F_2$ transitions based on the emission spectra (300 K) of the Eu^{3+} complexes and doped polymeric materials PMMA:[Eu(tta)$_3$(4-picNO)$_2$]x % and PMMA: [Eu(dbm)$_3$(4-picNO)]x % where x = 1, 3, 5, 10 and 15%

	Eu-tta	PET1	PET3	PET5	PET10	PET15	Eu-dbm	PED1	PED3	PED5	PED10	PED15
Ω2 (10^{-20}cm^2)	30	31	27	29	30	29	26	27	25	27	24	25
Ω4 (10^{-20}cm^2)	11	9	7	8	9	8	12	7	7	7	6	6

only dispersed into the polymeric matrix, though, of course, structural distortions may occur. Besides, emission spectral profiles of a particular Eu^{3+} (β-diketonate) complex (tta or dbm) are very similar compared with the respective doped polymer systems (Fig. 8), corroborating that the Eu^{3+} ion also act as powerful luminescence probe.

It is noted that know Ω_2 values of Eu^{3+}β-diketonate hydrated complexes [12] are within range of the Ω_2 values obtained after the coordination of the 4-picNO ligand. Since the substitution of water molecules of hydrated complexes by the 4-picNO ligand occur by the coordination of $O^{2-}Eu^{3+}$, there is little structural effect around the metal ions, resulting in similar Ω_2 values.

The photostability investigation of the luminescent materials $[Eu(tta)_3(4\text{-picNO})_2]$, $[Eu(dbm)_3(4\text{-picNO})]$ complexes as well as PMMA:$[Eu(tta)_3(4\text{-picNO})_2](10\%)$ and PMMA:$[Eu(dbm)_3(4\text{-picNO})](10\%)$ doped polymer films were evaluated (Fig. 9). Their emission spectra were recorded every 30 min for 2.5 h, under continuous exposure to UV irradiation at 394 nm, in the spectral range from 604 to 632 nm assigned to the $^5D_0 \rightarrow {}^7F_2$ transition. 450 W Xenon lamp was used as excitation source, which is much more intense than the UV radiation from the Sun.

Figure 9 illustrates that the photostability of the Eu^{3+} β-diketonate complex containing dbm and 4-picNO ancillary

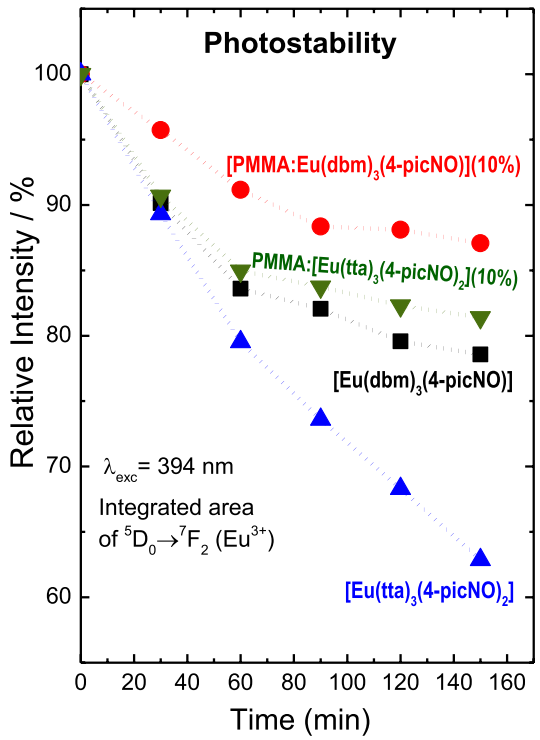

Fig. 9 Photostability curves of the $[Eu(tta)_3(4\text{-picNO})_2]$ and $[Eu(dbm)_3(4\text{-picNO})]$ complexes as well as for the PET10 and PED10 doped polymer films by using the integrated emission area of the $^5D_0 \rightarrow {}^7F_2$ transition (Eu^{3+})

ligand is higher compared to the tta ligand. In addition, the PED10 and PET10 doped polymeric films are more stable under UV irradiation than the individual europium complexes, indicating that PMMA:$[Eu(dbm)_3(4\text{-picNO})](10\%)$ doped film exhibit the highest photostability between the prepared luminescent materials [17, 25].

The higher photostability of PED10 and PET10 doped films than the individual complexes is probably due to the modification of the polymer surface and elimination of the defect within the texture/matrix after the UV light exposure, whereas for the Eu^{3+} ion, in the tta complex, the photodecomposition is the dominant process.

The question (mechanisms) of degradation, under UV (A, B or C) excitation of Ln^{3+} β-diketonates ligands, with ancillary ligands, is still an open question [25]. However, at least in the present case, we observe that the novel Eu^{3+} β-diketonate complexes with ancillary ligands as 4-picNO doped in PMMA films show considerably higher photostability then the complexes even under high power lamp UV-irradiation (450 W).

The CIE chromaticity diagram (*Commission internationale de l'éclairage*) illustrates the gradual spectral shifting of the Eu^{3+} complexes and doped PMMA polymeric materials [26], being directly related to emission spectral profiles and relative intensities of each samples (Fig. 10). By the CIE plot, it is possible to perceive a small shifting in (x,y) coordinates towards the reddish spectral region with increasing doped concentration of $[Eu(tta)_3(4\text{-picNO})_2]$ in polymeric films. This reddish shift is attributed to structural distortion around the metal ion, and possibly the nephelauxetic effect. Covalency effects, besides structural ones as mentioned, are certainly responsible for this observation. This is well discussed in references [27, 28]. Additionally, due to color tunneling, the PMMA doped films coordinates on the CIE slightly differ from the corresponding complexes due to small structural distortions around the metal ion.

Finally, it is possible to identify different $(2J+1)$ components of the $^5D_0 \rightarrow {}^7F_2$ transition with increasing concentration on the luminescence spectra of PMMA doped samples. Although these components do not alter Ω_2 values on a significant manner, their effects can be seen by the (x,y) coordinates shift presented in the CIE diagram.

4 Conclusion

Luminescent materials were successfully prepared by incorporation of the Eu^{3+}β-diketonate complexes in PMMA films by the solvent casting method, showing amorphous nature. SEM/EDS analysis revealed the effective dispersion of Eu^{3+}β-diketonate complexes throughout the polymer and the porous nature of PMMA. Furthermore,

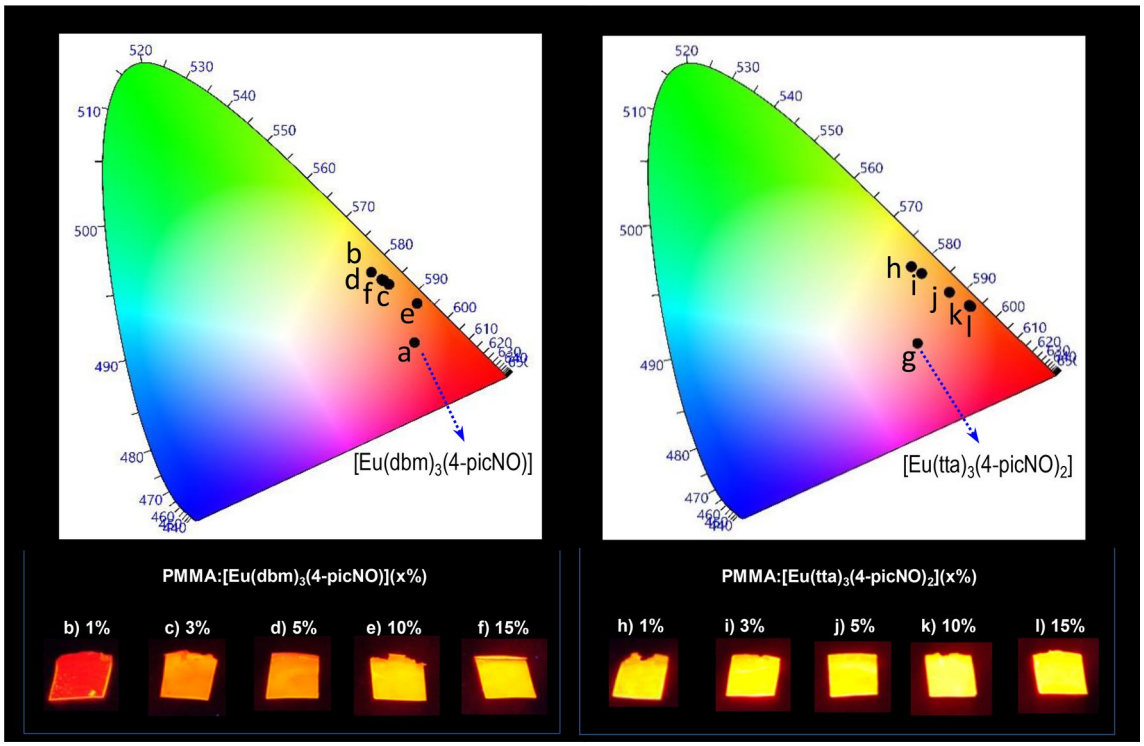

Fig. 10 CIE chromaticity diagrams showing the emission color tuning of PMMA:[Eu(tta)$_3$(4-picNO)$_2$](x %) and PMMA:[Eu(dbm)$_3$(4-picNO)](x %) doped film (x = 1, 3, 5, 10 and 15%). Photographs of the luminescent materials complexes taken with a digital camera displaying the reddish emissions under UV irradiation at 366 nm

VUV-UV synchrotron radiation excitation, absorption and excitation measurements indicated the distinction imposed by the PMMA and β-diketonate ligands (tta and dbm). Luminescence spectra of all samples exhibit only emission peaks assigned to the $^5D_0 \rightarrow {}^7F_J$ transitions of the Eu^{3+} ion with absence of phosphorescence of organic ligands, indicating efficient energy-transfer processes ligand–metal. The similar Ω_λ parameter values meaning that the Eu^{3+} complexes maintain their chemical and structural features in the first coordination sphere when doped in PMMA film, suggesting that there is a dispersion between Eu^{3+} complexes and polymeric matrix. The doped PMMA polymeric films exhibit higher photostability then the complexes even under high power lamp UV-irradiation. The CIE diagram also revealed a great similarity between the (x,y) coordinates for the PMMA doped samples compared to the corresponding β-diketonate complex, exhibiting the reddish color tuning.

Acknowledgements The authors thank the Brazilian Agencies: FAPESP, CAPES, CNPq, CNEN for financial support. Dr Veronica C. Teixeira, Dr Douglas Galante and Mr Leonardo M. Kofukuda (TGM beamline) from the Brazilian Synchrotron Light Laboratory, Brazilian Center for Research in Energy and Materials (LNLS and CNPEM), Campinas, SP, Brazil, are gratefully acknowledged for their assistance during vacuum UV-excited luminescence experiments.

References

1. J.-C.G. Bunzli, On the design of highly luminescent lanthanide complexes. Coord. Chem. Rev. **293–294**, 19–47 (2015)
2. L.D. Carlos, R.A.S. Ferreira, V. de Zea Bermudez, S.J.L. Ribeiro, Lanthanide-containing light-emitting organic–inorganic hybrids: a bet on the future. Adv. Mater. **21**(5), 509–534 (2009)
3. V.S. Sastri, J.C. Bunzli, J.R. Perumareddi, V.R. Rao, G.V.S. Rayudu, *Modern aspects of rare earths and their complexes* (Elsevier, Amsterdam, 2003)
4. B.K. Gupta, D. Haranath, S. Saini, V.N. Singh, V. Shanker, Synthesis and characterization of ultra-fine Y_2O_3:Eu^{3+} nanophosphors for luminescent security ink applications. Nanotechnology **21**(5), 055607 (2010)
5. J. Kido, H. Hayase, K. Hongawa, K. Nagai, K. Okuyama, Bright red light-emitting organic electroluminescent devices having an europium complex as an emitter. Appl. Phys. Lett. **65**(17), 2124–2126 (1994)
6. S. Heer, K. Kompe, H.U. Gudel, M. Haase, Highly efficient multicolour upconversion emission in transparent colloids of lanthanide-doped $NaYF_4$ nanocrystals. Adv. Mater. **16**(23–24), 2102–2105 (2004)
7. D.-C. Yu, R. Martín-Rodríguez, Q.Y. Zhang, A. Meijerink, F.T. Rabouw, Multi-photon quantum cutting in Gd_2O_2:Tm^{3+} to

enhance the photo-response of solar cells. Light **4**(10), e3441–e3448 (2015)
8. J.-C. Bunzil, S.V. Eliseeva, Lanthanide NIR luminescence for telecommunications, bioanalyses and solar energy conversion. J. Rare Earths **28**(6), 824–842 (2010)
9. A. Nadort, J. Zhaob, E.M. Goldys, Lanthanide upconversion luminescence at the nanoscale: fundamentals and optical properties. Nanoscale **8**(27), 13099–13130 (2016)
10. O.A. Savchuk, J.J. Carvajal, C.D.S. Brites, L.D. Carlos, M. Aguilo, F. Diaz, Upconversion thermometry: a new tool to measure the thermal resistance of nanoparticles. Nanoscale **10**(14), 6602–6610 (2018)
11. J.-C.G. Bunzil, Lanthanide light for biology and medical diagnosis. J. Lumin. **170**, 866–878 (2016)
12. G.F. Sá, O.L. Malta, C.D. Donega, A.M. Simas, R.L. Longo, P.A. Santa-Cruz, E.F. Silva Jr., Spectroscopic properties and design of highly luminescent lanthanide coordination complexes. Coord. Chem. Rev. **196**(1), 165–195 (2000)
13. H.F. Brito, O.L. Malta, M.C.F.C. Felinto, E.E.S. Teotonio, In patai series, in *The chemistry of metal enolates*, ed. by J. Zabicky (John Wiley & Sons Ltd, New Jersey, 2009), pp. 131–184
14. K. Binnemans, Interpretation of europium (III) spectra. Coord. Chem. Rev. **295**, 1–45 (2015)
15. P. Leanaerts, K. Driensen, R.V. Deun, K. Binnemans, Covalent coupling of luminescent Tris(2-thenoyltrifluoroacetonato) lanthanide(III) complexes on a merrifield resin. Chem. Mater. **17**(8), 2148–2154 (2005)
16. S. Biju, M.L.P. Reddy, A.H. Cowley, K.V. Vasudevan, 3-Phenyl-4-acyl-5-isoxazolonate complex of Tb^{3+} doped into poly-bhydroxybutyrate matrix as a promising light-conversion molecular device. J. Mater. Chem. **19**(29), 5179 (2009)
17. J. Kai, M.C.F.C. Felinto, L.A.O. Nunes, O.L. Malta, H.F. Brito, Intermolecular energy transfer and photostability of luminescence-tuneable multicolour PMMA films doped with lanthanide-β-diketonate complexes. J. Mater. Chem. **21**(11), 3796–3802 (2011)
18. Q.D. Ling, D.J. Liaw, C. Zhu, D.S.H. Chan, E.T. Kang, K.G. Neoh, Polymer electronic memories: materials, devices and mechanisms. Prog. Polym. Sci. **33**(10), 917–978 (2008)
19. S. Jana, A.S. Khojin, W.H. Zhong, H. Chen, X. Liu, Q. Huo, Effects of gold nanoparticles and lithium hexafluorophosphate on the electrical conductivity of PMMA. Solid State Ionics **178**(19–20), 1180–1186 (2007)
20. H. Althues, R. Palkovits, A. Rumplecker, P. Simon, W. Sigle, M. Bredol, U. Kynast, S. Kaskel, Synthesis and characterization of transparent luminescent ZnS:Mn/PMMA nanocomposites. Chem. Mater. **18**(4), 1068–1072 (2006)
21. S. Li, M.S. Toprak, Y.S. Jo, J. Dobson, D.K. Kim, Bulk synthesis of transparent and homogeneous polymeric hybrid materials with ZnO quantum dots and PMMA. Adv. Mater. **19**(24), 4347–4352 (2007)
22. S.C. Farmer, T.E. Pattern, Photoluminescent polymer/quantum dot composite nanoparticles. Chem. Mater. **13**(11), 3920–3926 (2001)
23. J. Gao, C. Lü, X. Lü, Y. Du, APhen-functionalized nanoparticles-polymer fluorescent nanocomposites via ligand exchange and in situ bulk polymerization. J. Mater. Chem. **17**(43), 4591–4597 (2007)
24. R. Chai, H. Lian, P. Yang, Y. Fan, Z. Hou, X. Kang, J. Lin, In situ preparation and luminescent properties of $LaPO_4$:Ce^{3+}, Tb^{3+} nanoparticles and transparent $LaPO_4$:Ce^{3+}, Tb^{3+}/PMMA nanocomposite. J. Colloid Interface Sci. **336**(1), 46–50 (2009)
25. T.A. Kovacs, M.C.F.C. Felinto, T.B. Paolini, B. Ali, L.K.O. Nakamura, E.E.S. Teotonio, H.F. Brito, O.L. Malta, Synthesis and photoluminescence properties of $[Eu(dbm)_3 \cdot PX]$ and $[Eu(acac)_3 \cdot PX]$ complexes. J. Lumin. **193**, 98–105 (2018)
26. C.S. Cunha, M. Köppen, H. Terraschke, G. Friedrichs, O.L. Malta, N. Stock, H.F. Brito, Luminescence tuning and single-phase white light emitters based on rare earth ions doped into a bismuth coordination network. J. Mater. Chem. C **6**, 2668–12678 (2018)
27. O.L. Malta, H.J. Batista, L.D. Carlos, Overlap polarizability of a chemical bond: a scale of covalency and application to lanthanide compounds. Chem. Phys. **282**, 21–30 (2002)
28. R.T. Moura Jr., O.L. Malta, R.L. Longo, The chemical bond overlap plasmon as a tool for quantifying covalency in solid state materials and its applications to spectroscopy. Int. J. Quantum Chem. **111**, 1626–1638 (2011)